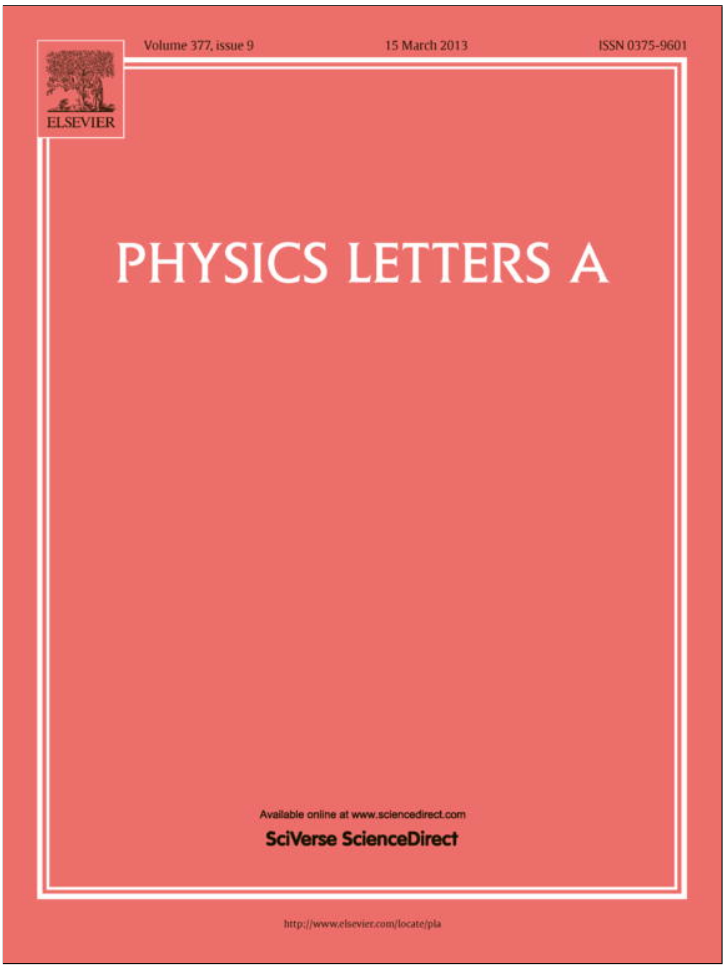

Physics Letters A 377 (2013) 721–726

Contents lists available at SciVerse ScienceDirect

Physics Letters A

www.elsevier.com/locate/pla

Phonon energy inversion in graphene during transient thermal transport

Jingchao Zhang [a], Xinwei Wang [a,*], Huaqing Xie [b]

[a] Department of Mechanical Engineering, 2010 Black Engineering Building, Iowa State University, Ames, IA 50011, USA
[b] School of Urban Development and Environmental Engineering, Shanghai Second Polytechnic University, Shanghai 201209, PR China

ARTICLE INFO

Article history:
Received 23 November 2012
Accepted 6 January 2013
Available online 16 January 2013
Communicated by R. Wu

Keywords:
Graphene
Phonon transport
Energy inversion
Localized phonon excitation
Static heat source

ABSTRACT

This work reports on the phonon energy inversion in graphene nanoribbons: after initial localized thermal excitation, the energy of initial cold phonons (flexural mode: FM) becomes higher than that of local hot phonons (longitudinal and transverse modes: LM/TM). Such energy inversion holds for about 50 picoseconds. Two physical factors combine together to give rise of this phenomenon: one is the much faster heat conduction by FM phonons than that by LM/TM phonons, and the other factor is the strongly temperature-dependent energy exchange rate between FM and LM/TM phonons: 3.7×10^{10} s^{-1} at 84 K to 20.3×10^{10} s^{-1} at around 510 K.

1. Introduction

Since its discovery, properties of graphene have been studied extensively due to their exotic electronic characteristics and realistic prospects of various applications [1–3]. Recent studies measured the lattice thermal conductivity of graphene at around 3000–5000 W/m K depending on the graphene flake size and temperature [4,5]. First principle calculations by Kong et al. [6] and Nika et al. [7] determined thermal conductivity values in the range of 2000–6000 W/m K. Using molecular dynamic (MD) simulations, several research groups [8–10] calculated graphene's thermal conductivity at a significantly lower range of 20–2000 W/m K depending on the width, roughness and edge type (armchair or zigzag) of the sample. Other carbon allotropes like graphite [11], carbon nanotubes (CNTs) [12–14] and diamond [15] also exhibit high thermal conductivity values because of the strong carbon atom bonding, which results in a large phonon contribution to its thermal conductivity.

Previous studies argued that the thermal conductivity in single layer graphene (SLG) is mainly contributed to by the in-plane transverse (TA) and longitudinal acoustic (LA) phonons, while the out-of-plane flexural acoustic (ZA) phonon contribution can be ignored due to its small group velocity [7]. However, recent research shows that for a suspended SLG, the ZA phonon modes can contribute as much as 77% at 300 K and 86% at 100 K of the thermal conductivity due to the high specific heat and a longer mean phonon scattering time [16]. By formulating the ballistic thermal conductance of phonons in a two-dimensional system and using the phonon's dispersion relation, Nakamura et al. [17] calculated the contributions of the TA, LA and ZA phonons to graphene's thermal conductance. They conclude that the ballistic phonon conductance is determined by the ZA phonon modes below about 20 K and contributions of the TA and LA phonon modes cannot be neglected above 20 K while the ZA phonon contribution is still dominant. Besides, by numerically solving the phonon Boltzmann equation, Lindsay et al. [18] came up with a symmetry-based selection rule which significantly restricts anharmonic phonon–phonon scattering of the ZA phonons and they prove that the lattice thermal conductivity of SLG is dominated by the ZA phonon modes.

Thus far, the reported high thermal conductivity of FM phonons has sparked a keen interest in the study of graphene's thermal properties. Here we represent an energy inversion phenomenon observed in the transient thermal transport in GNR system. Phonon energy coupling among different phonon modes is investigated systematically and it is found that both dynamic and static heat sources can evoke the energy inversion in GNR. Our preliminary speculation for this novel property of graphene can be summarized into two aspects. One is the much higher thermal conductivity of FM phonons than that of TM/LM phonons. The other one is that the energy coupling between FM and TM/LM phonons is not constant against their energy level: the coupling becomes stronger when the phonon energy is higher. The above speculations are

* Corresponding author. Tel.: +1 515 294 2085; fax: +1 515 294 3261.
E-mail address: xwang3@iastate.edu (X. Wang).

0375-9601/$ – see front matter
http://dx.doi.org/10.1016/j.physleta.2013.01.013

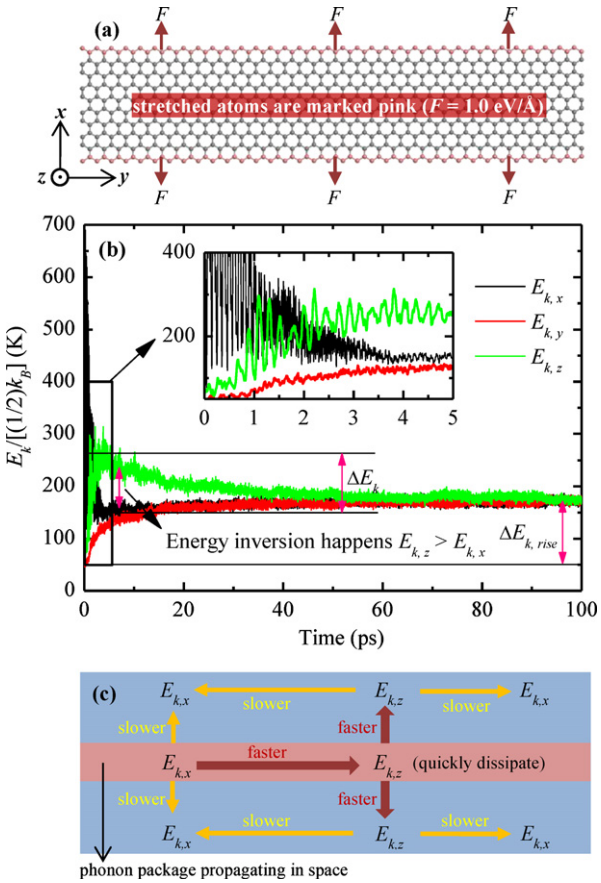

Fig. 1. Atomic configuration and energy inversion characterization in the 2.0 × 25.0 ($x \times y$) nm^2 GNR system. (a) Periodic boundary condition is applied to the y direction and free boundary conditions are applied to the x and z directions. The two outermost layers of atoms in the x direction (marked as pink) are grouped to apply the stretching force ($F = 1.0$ eV/Å). This coordinate system is used for all the discussions in this work. (b) The $E_{k,x}$, $E_{k,y}$ and $E_{k,z}$ profiles of the GNR after 25 fs phonon excitation at the boundary. (c) The $E_{k,x}$ and $E_{k,z}$ energy exchange after the GNR is stretched in the width direction. The red area represents phonon package propagations induced by the stretch. (For interpretation of the references to color in this figure legend, the reader is referred to the web version of this Letter.)

explained and elaborated in the following discussions in Sections 2.1 to 2.3. Energy inversion in multilayer graphene is studied in Section 2.4.

2. Results and discussion

2.1. Phonon energy inversion after localized phonon excitation

First of all, we study the phonon energy evolution after localized phonon excitation in a graphene nanoribbon (GNR) as shown in Fig. 1a. A single layer GNR with dimensions of 2.0 × 25.0 nm^2 ($x \times y$) is constructed. The second generation of the Brenner potential [19]: reactive empirical bond-order (REBO), based on the Tersoff potential [20,21] with interactions between C–C bonds is applied in our MD simulation reported in this Letter. Periodic boundary condition is applied to the y direction and free boundary conditions are applied to the x and z directions. To compare the energy evolution of different phonon modes and the whole system, a quantity defined as $E_k/[(1/2)k_B]$, where E_k is kinetic energy and k_B is the Boltzmann constant, with unit K is used to represent the energy values in each direction and a value $E_k/[(3/2)k_B]$ with unit K stands for the system's total energy. "Bias" has been removed from the atomic velocities when energies are calculated.

During initial system equilibrium calculation, a time step of 0.5 fs (1 fs = 10^{-15} s) is used. After 150 ps (1 ps = 10^{-12} s) energy equilibrium calculation, the system reaches the expected steady state at 50 K. Then two layers of carbon atoms at each end in the x direction are grouped to apply opposite stretching forces (F) to each atom for 25 fs. The stretching force is 1.0 eV/Å per atom. Atomic structure of the system is depicted in Fig. 1a. The GNR system is left to relax for the next 100 ps until it reaches energy equilibrium again. The time step is reduced to 0.05 fs in these phonon excitation and relaxation processes in anticipation to capture detailed phonon energy evolution.

Due to the displacement of the outermost carbon atoms, a phonon package is excited and propagates to the inside from each boundary in the x direction. Temperatures of the path through which the phonon package propagates will become higher than the rest areas, which gives rise to moving local hot regions in the GNR. Due to the phonon excitation in the x direction, the average energy of the system increases from 50 K to 194 K immediately after excitation. To take a closer look at the energy relaxation process, energies of phonons in all three directions ($E_{k,x}$, $E_{k,y}$, $E_{k,z}$) are computed and shown in Fig. 1b. The results are averaged every 100 steps to suppress the data noise. At the end of excitation, $E_{k,x}$, $E_{k,y}$ and $E_{k,z}$ are 478 K, 48 K and 57 K respectively. This clearly shows that the excitation almost solely increases the energy of phonons in the x direction while the y and z mode phonons stay cold. Since the energy of the longitudinal phonons ($E_{k,x}$) is much higher than the other two modes ($E_{k,y}$, $E_{k,z}$), energy exchange among the three phonon branches will occur continuously until the GNR system reaches energy equilibrium again.

Generally, one would expect in such scenario $E_{k,y}$ and $E_{k,z}$ will increase gradually, and $E_{k,x}$ will decrease until the three phonon mode energies reach the same level. However, according to our calculated results, the longitudinal phonon energy ($E_{k,x}$) decreases dramatically at the beginning of the relaxation procedure while the flexural phonon energy ($E_{k,z}$) rises much faster than the transverse phonon energy ($E_{k,y}$) and becomes higher than $E_{k,x}$ at around 2.0 ps. It is seen that the energy exchange between $E_{k,x}$ and $E_{k,y}$ does not give rise to such inversion phenomenon, and they reach the same level after about 15 ps. On the other hand, at the moment $E_{k,z}$ reaches its peak value, $E_{k,x}$ also reaches its minimum, and the energy inversion ($E_{k,x} - E_{k,z}$) reaches the highest level. Then energy flows back from $E_{k,z}$ to $E_{k,x}$ and $E_{k,y}$, and it takes a much longer time (~ 50 ps) for them to reach the same level. This points out that the energy exchange between $E_{k,x}$ and $E_{k,z}$ is much slower than that between $E_{k,x}$ and $E_{k,y}$, agreeing with our previous observation in studying the temporal response of a GNR to a thermal impulse [10].

First of all, for this first-time observed surprising behavior in graphene, our speculation of the driving force behind it is the much higher thermal transport capability by the flexural (z) mode phonons. As illustrated in Fig. 1c, phonon energies in the moving local hot regions of GNR will increase dramatically when the phonon package propagates in the lateral direction. This high local energy will induce a high local $E_{k,z}$. According to Lindsay et al. [18], for a suspended SLG, the ZA phonon mode has a large density of states and follows a selection rule for anharmonic phonon scattering, which contributes to its anomalously large thermal conductivity. Therefore, due to the large thermal conductivity of ZA phonons, the local flexural mode energy ($E_{k,z}$) will dissipate in space very fast, which allows the local $E_{k,x}$ to always remain higher than $E_{k,z}$. Consequently in the local hot regions, thermal energy keeps flowing from $E_{k,x}$ to $E_{k,z}$, while in the whole GNR system $E_{k,z}$ becomes greater than $E_{k,x}$. One argument is that in regions where $E_{k,z} > E_{k,x}$, energy will flow back from $E_{k,z}$ to $E_{k,x}$, and offset the energy flow from $E_{k,x}$ to $E_{k,z}$ in the regions of $E_{k,x} > E_{k,z}$. We will prove later that this energy flow back is

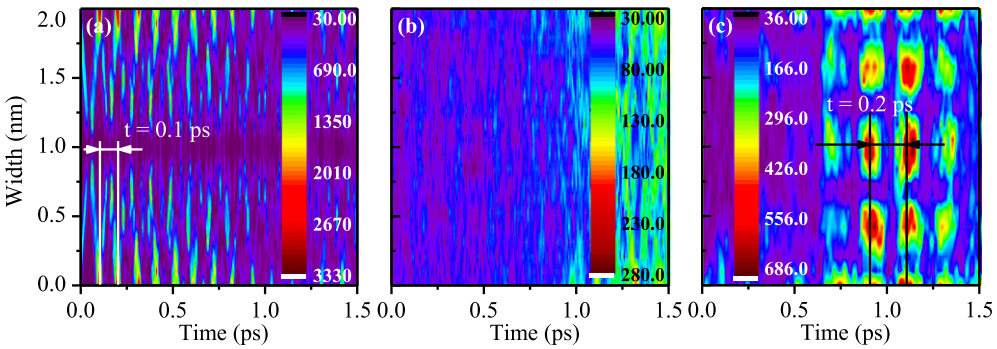

Fig. 2. Phonon package propagations in the width direction of the 2.0×25.0 $(x \times y)$ nm^2 GNR system. (a), (b) and (c) are for the spatial-energy contours of $E_{k,x}$, $E_{k,y}$ and $E_{k,z}$ respectively.

much slower due the fact that the $E_{k,x} - E_{k,z}$ coupling is weaker when the local temperature is lower [Fig. 1c]. Energy transfer rates among the three mode phonons will be discussed below to give detailed physical analysis of this process.

2.2. Phonon package propagation and phonon coupling

From the inset of Fig. 1b we clearly see that $E_{k,x}$ decreases in a sinusoidal pattern (oscillating). This is caused by the phonon package traveling and reflections at the x boundaries. To better analyze the phonon package propagation and energy exchange in the GNR, we plot its spatiotemporal contours in respect of $E_{k,x}$, $E_{k,y}$ and $E_{k,z}$ in Figs. 2a, b and c respectively. The results are presented without any data average. It can be seen that the longitudinal (x) phonon packages are traveling between the two x boundaries and the wave amplitude decays with time due to the energy transfer and phonon scattering. The propagation speed of the longitudinal phonon package is calculated at 19.9 km/s. The local energies at the boundary where the phonons are reflected are higher than those at the other places due to the overlap of incident and reflection waves which amplifies the wave amplitude. The local energies in the center are lower since the phonon packages from opposite directions cancel out and weaken the local lattice vibration. No transverse (y) phonon package propagation is observed in Fig. 2b. In Fig. 2c, flexural (z) phonon package propagation is observed. In Fig. 2a, we calculate the period of the longitudinal phonon package to be 0.1 ps, corresponding to a phonon moving back and forth frequency of 10 THz. In Fig. 2c, the period for the flexural phonon package is calculated at 0.2 ps, which corresponds to a phonon moving back and forth frequency of 5 THz.

We developed a speculation that the energy inversion in GNR is caused by phonon package propagations, which create moving hot local regions where the thermal energies keep transferring from the in-plane to out-of-plane phonons until the phonon package dies out. The key point for such energy inversion is very localized phonon excitation. Therefore if there is no phonon package generated in the GNR system, the energy inversion should not be observed among $E_{k,x}$, $E_{k,y}$ and $E_{k,z}$. To test this point, we use a 2.0×25.0 nm^2 $(x \times y)$ GNR to investigate the energy transfer among the three phonon branches without inducing any phonon propagation influence. The GNR system is initially placed in a Nose–Hoover [22,23] thermal bath for 200 ps until the system reaches energy equilibrium at 50 K. Then the velocity of atoms in the x direction (v_x) is rescaled to two times their original values. Therefore according to the energy equipartition theorem, the x mode phonon energy ($E_{k,x}$) will become four times the initial value, which is around 200 K in this case. Due to the increase of $E_{k,x}$, thermal energies will be transferred to $E_{k,y}$ and $E_{k,z}$, and no phonon package is generated since the GNR is heated uniformly in the x direction. The energy relaxation process is shown in Fig. 3a.

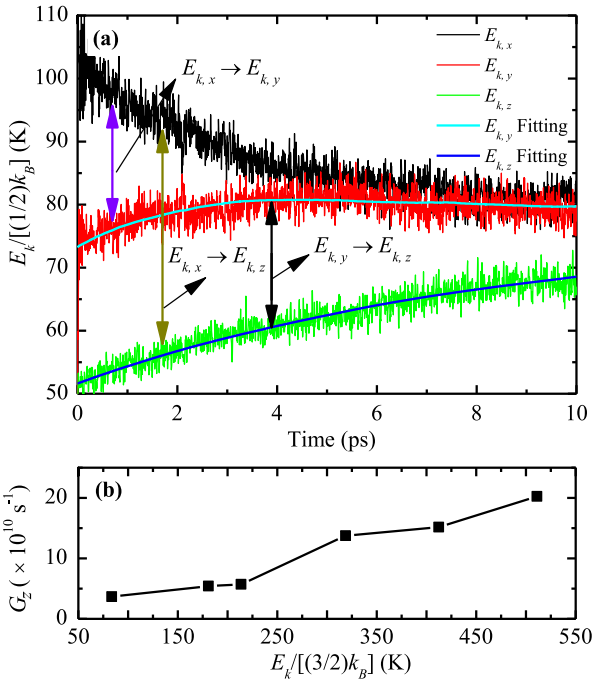

Fig. 3. Calculation of phonon coupling time against energy. (a) Energy evolutions after $E_{k,x}$ is rescaled to ~ 200 K. (b) The characteristic coupling time of the in-plane phonons and the flexural phonons at different energy levels. It is conclusive G_z increases with the local energy level, meaning if the phonon is more excited, the mode-wide coupling will be stronger.

The time step is 0.05 fs during the relaxation and the results are averaged every 100 steps to suppress the data noise. Compared with Fig. 1b, it is seen that no energy inversion happens between in-plane and out-of-plane phonon energies.

In Fig. 3a, three energy transfer processes are observed, which are $E_{k,x} \rightarrow E_{k,z}$, $E_{k,y} \rightarrow E_{k,z}$ and $E_{k,x} \rightarrow E_{k,y}$ respectively. The evolution of $E_{k,z}$ can be expressed as

$$\frac{\partial E_{k,z}}{\partial t} = G_{xz}(E_{k,x} - E_{k,z}) + G_{yz}(E_{k,y} - E_{k,z}), \tag{1}$$

where G_{xz}, G_{yz} are the inverse values of the coupling time for $E_{k,x} \rightarrow E_{k,z}$ and $E_{k,y} \rightarrow E_{k,z}$. Since $E_{k,x}$ and $E_{k,y}$ are both in-plane phonon energies, to simplify the coupling analysis we assume their coupling times with $E_{k,z}$ are the same ($G_{xz} = G_{yz} = G_z$). The theoretical basis of Eq. (1) could be explained by the following. After the v_x rescaling, the total energy of the system remains constant while $E_{k,x}$, $E_{k,y}$ and $E_{k,z}$ are different, i.e., there is no spatial heat conduction in the system but energy transfer among different phonon modes. The change in certain phonon energy is only caused by its coupling with other phonon modes. The phonon en-

ergy exchange happens as long as there are energy differences among them. Take $E_{k,z}$ as an example, the change of $E_{k,z}$ is caused by its coupling with $E_{k,x}$ and $E_{k,y}$. To describe this change, coefficients of G_{xz} and G_{yz} with unit s^{-1} are introduced to characterize the coupling rate of $E_{k,z}$ with $E_{k,x}$ and $E_{k,y}$ respectively. Then the evolution of $E_{k,z}$ can be described by calculating the time integration of its coupling rate with $E_{k,x}$ and $E_{k,y}$. Since $E_{k,z}$ is already given by the MD simulation results, G_z can be determined by best fitting the MD results using Eq. (1). Given a proper G_z value, Eq. (1) could be used to fully describe the evolution of $E_{k,z}$. By fitting the MD simulation data of $E_{k,z}$ with numerical results calculated from Eq. (1) using the least square method, we calculate the G_z value at 3.96×10^{10} s^{-1}, corresponding to a coupling time (τ_z) of 25.3 ps. Similarly, the equation for the evolution of $E_{k,y}$ is

$$\frac{\partial E_{k,y}}{\partial t} = G_{xy}(E_{k,x} - E_{k,y}) + G_z(E_{k,z} - E_{k,y}), \tag{2}$$

where G_{xy} is the inverse of the coupling time between $E_{k,x}$ and $E_{k,y}$. Given $G_z = 3.96 \times 10^{10}$ s^{-1}, the value of G_{xy} is calculated at 1.86×10^{11} s^{-1} based on data fitting of the $E_{k,y}$ evolution, and the phonon relaxation time (τ_{xy}) is 5.4 ps. From the above results, we can see that τ_z is 4.7 times τ_{xy}, meaning the energy transfer for $E_{k,x} \to E_{k,z}$ and $E_{k,y} \to E_{k,z}$ are much slower than that between $E_{k,x}$ and $E_{k,y}$.

According to the previous study by Lee et al. [24], the thermal conductivity of graphene decreases with temperature. It is expected the characteristic coupling time between in-plane and out-of-plane phonons will decrease with time, which should lead to an increasing G_z value against temperature in graphene. Therefore we also conducted a study on how the phonon coupling constant G_z changes with the local energy level (temperature). For this study, we rescale $E_{k,x}$ and $E_{k,y}$ simultaneously to the same value and use Eq. (1) to calculate G_z. The G_z values at different energies are shown in Fig. 3b. We can see that G_z increases with temperature, from around 3.7×10^{10} s^{-1} at 84 K to 20.3×10^{10} s^{-1} at around 510 K. This indicates that the thermal energy transport between the in-plane and out-of-plane phonons becomes faster as temperature increases, meaning the phonon coupling between $E_{k,x}/E_{k,y}$ and $E_{k,z}$ in hot local regions is stronger than that in cold regions. From the above discussions, we conclude that the energy inversion in GNR is mainly caused by two reasons. First, the out-of-plane phonons make substantial contribution to the GNR's thermal conductivity and dissipate heat much faster than the in-plane phonons. Second, in the moving hot local regions where the phonon package passes by, the coupling time between in-plane and out-of-plane phonons is much smaller than that in the cold area. This leads to a continuous net energy transfer from $E_{k,x}/E_{k,y}$ to $E_{k,z}$.

From the above work, we have learned that energy inversion will happen when a phonon package is excited in the x direction. However, since the thermal conductivity and phonon boundary scattering rate in the x and y directions are different, it is necessary to further examine the phonon energy evolution when the phonon package is excited in the y direction. A 2.0×25.0 nm^2 ($x \times y$) flat GNR is built to reach thermal equilibrium at temperature 50 K. Periodic boundary condition is applied to the x direction and free boundary conditions are applied to the y and z directions. Then two layers of carbon atoms at one end in the y direction are grouped to apply a stretching force (F in the y direction) for 25 fs. The stretching force is 5.0 eV/Å per atom. Atomic structure of the system is shown in the inset of Fig. 4. Phonon energy evolutions in each direction are shown in Fig. 4. The time step is 0.05 fs during the relaxation and the results are averaged every 100 steps to suppress the data noise. It is observed that right after the phonon package excitation, $E_{k,y}$ becomes higher than $E_{k,x}$ and $E_{k,z}$. Then at ~ 18 ps, $E_{k,z}$ exceeds $E_{k,y}$ to become the highest, which indicates the occurrence of energy inversion. An energy bump at ~ 1.25 ps is observed in the $E_{k,y}$ profile. The energy bump is induced by the longitudinal phonon package's reflection on the other end in the y direction, which increases the atoms' kinetic energy in the local area. Based on the appearance time of this energy bump, the longitudinal phonon package speed is calculated at 20.0 km/s, which is nearly the same with previous result of 21.3 km/s [25].

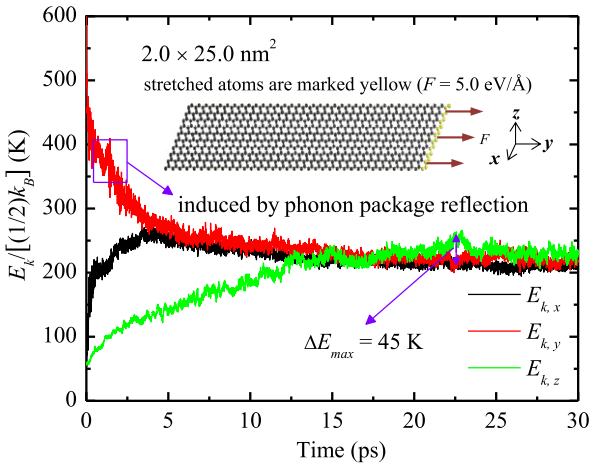

Fig. 4. Energy inversion characterization in the GNR system with phonon package excitation in the y direction. Periodic boundary condition is applied to the x direction and free boundary conditions are applied to the y and z directions. Two outermost layers of carbon atoms at the right end (marked as yellow) are grouped to apply stretching force ($F = 5.0$ eV/Å). An energy bump is observed in the $E_{k,y}$ profile, which is induced by the phonon package reflection on the graphene boundary. (For interpretation of the references to color in this figure legend, the reader is referred to the web version of this Letter.)

2.3. Energy inversion with a static heat source

From the above physics analysis, we predict that phonon energy transfer and exchange caused by a static localized heating source will also induce energy inversion in a GNR system. To prove our prediction, a 2.0×125.1 nm^2 ($x \times y$) GNR system is built [Fig. 5d]. The outermost layer of carbon atoms at each end in the y direction are fixed to avoid the spurious global rotation of the GNR and free boundary conditions are applied to the x and z directions. The system initially reaches thermal equilibrium at 50 K. Then a region of 2.0×25.0 nm^2 [region B shown in Fig. 5d] at the left end of the GNR is exposed to a thermal impulse. The heating time is 2 fs and the final temperature in the heating region is 619 K. Figs. 5a, b and c show the energy evolutions of the whole system, region A and region B. The time step is 0.5 fs during the relaxation and the results are averaged every 10 steps to suppress the data noise. First and most importantly, energy inversion is observed in Fig. 5a. At around 5 ps, the flexural mode (FM) phonon energy ($E_{k,z}$) becomes higher than those of the transverse mode (TM) ($E_{k,x}$) and longitudinal mode (LM) ($E_{k,y}$) phonons. It can be seen from Fig. 5c that in region B, $E_{k,z}$ decreases faster than $E_{k,x}$ and $E_{k,y}$. This is because the FM phonon carries more heat to the low energy region (region A) than the TM and LM phonons due to the much higher thermal conductivity sustained by FM phonons. As a result, $E_{k,z}$ in region A is higher than $E_{k,x}$ and $E_{k,y}$ due to the continuous heat current from region B by FM phonons, which is clearly shown in Fig. 5b. In region B, the LM and TM phonons keep transferring thermal energy to the FM phonons due to the energy difference between them, as shown in the inset of Fig. 5c. This continuous heat transfer between the in-plane phonons and out-of-plane phonons eventually causes higher total energies in

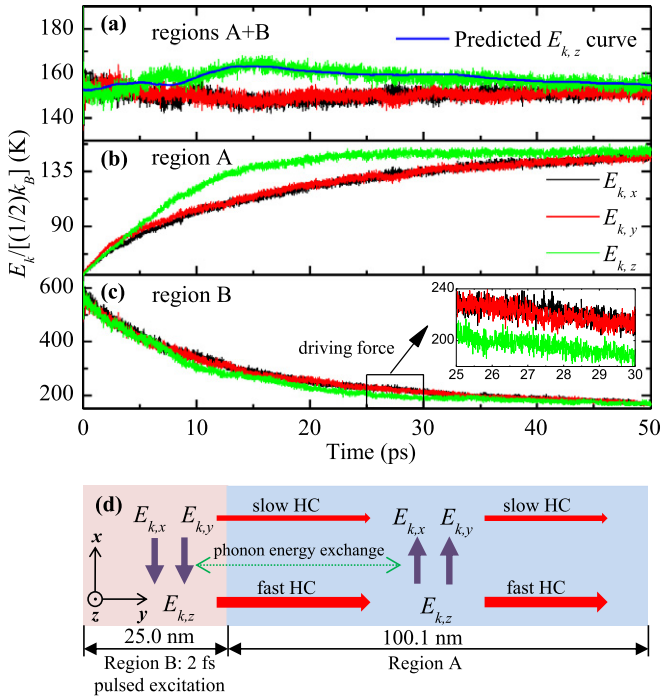

Fig. 5. Energy inversion characterization with static heating source. Fixed boundary condition is applied to the y direction and free boundary conditions are applied to the x and z directions. (a), (b) and (c) show energy evolutions of the whole region, region A, and region B. (d) Schematic to show the phonon transport in the 2.0×125.1 $(x \times y)$ nm^2 GNR. Heat conduction (HC) among FM phonons is much faster than those among LM and TM phonons. The red area (region B) is the 25.0 nm heating region where $E_{k,x}$ and $E_{k,y}$ transfer to $E_{k,z}$. The thermal energies will mainly be transported by $E_{k,z}$ to the low energy area (region A) where $E_{k,z}$ mostly transfers to itself in space (heat conduction) and partially to $E_{k,x}$ and $E_{k,y}$. (For interpretation of the references to color in this figure legend, the reader is referred to the web version of this Letter.)

the z direction and induces energy inversion in GNR. During the heat conduction from region B to region A, the FM phonons will largely transfer their energy to FM phonons (heat conduction), and transfer very little to the LM and TM phonons. One argument is that in region A, the FM phonons have a higher energy than the LM and TM phonons, so the energy could be transferred from FM phonons to LM and TM phonons in this region. This could prevent the energy inversion from happening. The fact is that in region B, the local energy is higher and will lead to faster LM/TM to FM phonon energy transfer (smaller coupling time). In region A, the local energy is low, and the energy transfer from FM to LM and TM phonons is slow (longer coupling time). Therefore, more energy will stay in the FM phonons, leading to energy inversion.

The energy transport rate from the TM and LM phonons to the FM phonons in region B is expressed as

$$E'_{z,in} = G_{z1}(E_{k,x} - E_{k,z}) + G_{z1}(E_{k,y} - E_{k,z}), \tag{3}$$

where $E_{k,x}, E_{k,y}, E_{k,z}$ are the phonon energies in the 25.0 nm region. Similarly, the energy transport rate from the FM phonons to the TM and LM phonons in region A can be written as

$$E'_{z,out} = G_{z2}(E_{k,z} - E_{k,x}) + G_{z2}(E_{k,z} - E_{k,y}). \tag{4}$$

The differences between $E'_{z,in}$ and $E'_{z,out}$ will be the rate of energy accumulating in the flexural phonons. The FM phonon energy profile of the whole system can be predicted as

$$E_{k,z} = \frac{V_B \int E'_{z,in}\,dt - V_A \int E'_{z,out}\,dt}{V_{GNR}}, \tag{5}$$

where V_A, V_B and V_{GNR} represent the volume of region A, region B and the entire GNR respectively. The G_{z1} and G_{z2} values will change with energy as shown in Fig. 3b, while in this case we simplify the calculation by using $G_{z1} = 22 \times 10^{10}$ s^{-1} and $G_{z2} = 4.15 \times 10^{10}$ s^{-1} at the average FM energy for the time range 0–15 ps, and $G_{z1} = 14.5 \times 10^{10}$ s^{-1} and $G_{z2} = 5.3 \times 10^{10}$ s^{-1} for the time range 15–50 ps. By substituting $E_{k,x}, E_{k,y}$ and $E_{k,z}$ values into Eqs. (3)–(5), the predicted $E_{k,z}$ values are plotted in Fig. 5a (blue solid curve). It is very exciting to observe that the predicted $E_{k,z}$ curve soundly matches the MD simulation results. This strongly proves that the input energy to the FM phonons is greater than the output energy, therefore inducing energy inversion in GNR. Also this prediction quantitatively proves the physics we proposed for the energy inversion phenomenon.

2.4. Energy inversion in multilayer graphene

Klemens [26,27] clearly distinguished the thermal transport in SLG and in bulk graphite. In the latter case there appears strong coupling within the cross-plane phonon modes and heat propagates in all directions, which reduces the contributions to heat conduction of the low-energy modes along the basal planes to negligible. By following the spirit of Klemens [26,27], Balandin et al. [7] proved that thermal conductivity of bulk graphite is much lower than that of single layer graphene. According to Lindsay et al. [28], the interaction between graphene layers breaks the selection rule on phonon–phonon scattering and results in a reduced thermal conductivity in the ZA phonon mode. As a result, we expect that the energy inversion in GNR will also be weakened in multilayer graphene (MLG).

For the MLG systems studied in this work, the interaction between graphene layers is described by the Lennard-Jones (LJ) potential as

$$v_{LJ}(r) = 4\varepsilon\left[\left(\frac{\sigma}{r}\right)^{12} - \left(\frac{\sigma}{r}\right)^{6}\right], \tag{6}$$

where r is the distance between carbon atoms and ε and σ are the common LJ parameters, which are set to be 0.0046 eV and 3.3276 Å respectively. Only the coupling between adjacent graphene planes is included in all the systems. Dimension of the MLG system is 2.0 nm × 25.0 nm $(x \times y)$, with n number of graphene layers in the z direction. Coordinates and boundary conditions of the system are the same as those displayed in Fig. 1a. A time step of 0.5 fs is used along the whole calculation. After energy equilibrium calculation at 50 K, the MLG system is stretched in the x direction (2.0 nm side direction) with two opposite forces (1.0 eV/Å per atom) applied on each side for 25 fs. Only the outmost two layers of atoms at each end in the x direction are stretched, like the scenario shown in Fig. 1a. After the stretching process, energy relaxation is performed for the next 100 ps. Energy changes in all three phonon modes are calculated during the relaxation process and the results for $N = 1, 4, 7, 10$ MLGs are shown in Figs. 6a, b, c and d. The results are presented without any data average. We can see from these figures that as the layer number increases, the maximum $E_{k,z}$ decreases and energy inversion is weakened. To be more specific, we calculate the $E_{k,z}$ difference between the initial and the final state as the denominator ($\Delta E_{k,rise}$) and the difference between the peak $E_{k,z}$ value and the minimum $E_{k,x}$ value as the nominator (ΔE_k). The ΔE_k and $\Delta E_{k,rise}$ value definition is denoted in Fig. 1b. ΔE_k is the maximum energy inversion between $E_{k,z}$ and $E_{k,x}$, and $\Delta E_{k,rise}$ is the final system energy rise induced by the initial phonon excitation. The ratio reflects the strength of the energy inversion process and their values are plotted in Fig. 6e. The $\Delta E_k/\Delta E_{k,rise}$ values decrease with an increasing layer number, which further proves that the energy inversion is weakened as layer numbers increase. This weakening

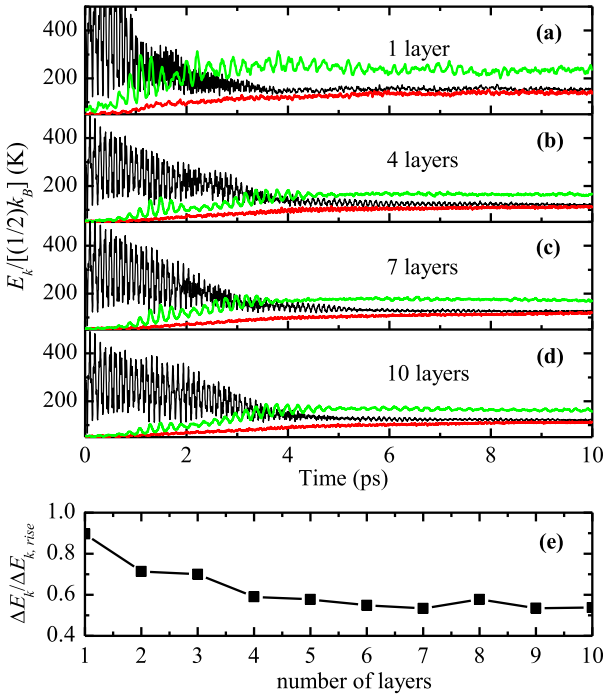

Fig. 6. Damping energy inversion against growing layers. (a), (b), (c) and (d) show energy evolutions for graphene with different layer numbers. The black, red and green solid lines represent $E_{k,x}$, $E_{k,y}$ and $E_{k,z}$ respectively. (e) $\Delta E_k/\Delta E_{k,rise}$ with different layer numbers from 1 to 10. Definitions of ΔE_k and $\Delta E_{k,rise}$ are illustrated in Fig. 1b. (For interpretation of the references to color in this figure legend, the reader is referred to the web version of this Letter.)

is most obvious when the graphene layer number changes from 1 to 2, and is moderate with further layer number increases. We conclude from Fig. 6e that energy inversion is weakened due to a reduced FM mode thermal conductivity in the MLG. Due to the computational cost for multilayer graphene, our calculations only include layer thickness ranges from 1 to 10. However, for much thicker ones, we expect the energy inversion phenomenon will still exist but be much weaker. We believe this is an intrinsic property of graphite. However, this energy inversion phenomenon is not a 2-D effect. To observe the energy inversion at the system level, the material must have strong mode-wide non-uniform thermal conductivity and temperature-dependent inter-mode energy coupling rate.

3. Conclusion

In summary, energy inversion in a GNR system during transient thermal transport was observed. The observed energy inversion requires localized phonon excitation (single mode or mode-wide) and can hold for about 50 ps. There are two main factors that contribute to the energy inversion in GNR. One is the much higher thermal conductivity of FM phonons than that of TM/LM phonons. The other one is that the energy coupling between FM and TM/LM phonons is not constant against their energy level: the coupling becomes stronger when the phonon energy is higher. Under the influence of a moving or static localized heat source, the FM phonons conduct heat much faster than the LM/TM phonons. Consequently thermal energy continuously transfers from LM/TM phonons to FM phonons in the heat source region while in the cold region the energy flow-back is much slower. We conducted prediction of energy inversion and the results agreed very well with the MD observation. With an increasing layer number of graphene, the energy inversion was weakened due to a decreasing thermal conductivity of FM phonons. Our observation points out a novel way for temporal energy storage in FM phonons, and energy conversion from LM/TM to FM mode (energy separation and isolation).

Acknowledgements

Partial support of this work from the National Science Foundation (Grants No. CBET-0931290, No. CMMI-1029072, No. CBET-0932573, and No. CMMI-0926704) is gratefully acknowledged. We thank Dr. Xiaopeng Huang for helpful discussions. H.X. thanks the great support from National Science Foundation of China (51176106). X.W. and H.X. also thank the support by the Eastern Scholar Program of Shanghai, China.

References

[1] A.H. Castro Neto, F. Guinea, N.M.R. Peres, K.S. Novoselov, A.K. Geim, Rev. Modern Phys. 81 (2009) 109.
[2] A.K. Geim, Science 324 (2009) 1530.
[3] Y.N. Yue, J.C. Zhang, X.W. Wang, Small 7 (2011) 3324.
[4] A.A. Balandin, S. Ghosh, W.Z. Bao, I. Calizo, D. Teweldebrhan, F. Miao, C.N. Lau, Nano Lett. 8 (2008) 902.
[5] S. Ghosh, I. Calizo, D. Teweldebrhan, E.P. Pokatilov, D.L. Nika, A.A. Balandin, W. Bao, F. Miao, C.N. Lau, Appl. Phys. Lett. 92 (2008) 151911.
[6] B.D. Kong, S. Paul, M.B. Nardelli, K.W. Kim, Phys. Rev. B 80 (2009) 033406.
[7] D.L. Nika, S. Ghosh, E.P. Pokatilov, A.A. Balandin, Appl. Phys. Lett. 94 (2009) 203103.
[8] W.J. Evans, L. Hu, P. Keblinski, Appl. Phys. Lett. 96 (2010) 203112.
[9] Z.X. Guo, D. Zhang, X.G. Gong, Appl. Phys. Lett. 95 (2009) 163103.
[10] J.C. Zhang, X.P. Huang, Y.N. Yue, J.M. Wang, X.W. Wang, Phys. Rev. B 84 (2011) 235416.
[11] G.A. Slack, Phys. Rev. 127 (1962) 694.
[12] P. Kim, L. Shi, A. Majumdar, P.L. McEuen, Phys. Rev. Lett. 87 (2001) 215502.
[13] E. Pop, D. Mann, J. Cao, Q. Wang, K. Goodson, H.J. Dai, Phys. Rev. Lett. 95 (2005) 155505.
[14] C.H. Yu, L. Shi, Z. Yao, D.Y. Li, A. Majumdar, Nano Lett. 5 (2005) 1842.
[15] G.A. Slack, J. Appl. Phys. 35 (1964) 3460.
[16] J.H. Seol, I. Jo, A.L. Moore, L. Lindsay, Z.H. Aitken, M.T. Pettes, X.S. Li, Z. Yao, R. Huang, D. Broido, N. Mingo, R.S. Ruoff, L. Shi, Science 328 (2010) 213.
[17] K. Saito, J. Nakamura, A. Natori, Phys. Rev. B 76 (2007) 115409.
[18] L. Lindsay, D.A. Broido, N. Mingo, Phys. Rev. B 82 (2010) 115427.
[19] D.W. Brenner, O.A. Shenderova, J.A. Harrison, S.J. Stuart, B. Ni, S.B. Sinnott, J. Phys., Condens. Matter 14 (2002) 783.
[20] B.W. Dodson, Phys. Rev. B 35 (1987) 2795.
[21] J. Tersoff, Phys. Rev. Lett. 61 (1988) 2879.
[22] W.G. Hoover, Phys. Rev. A 31 (1985) 1695.
[23] S. Nose, Mol. Phys. 52 (1984) 255.
[24] J.U. Lee, D. Yoon, H. Kim, S.W. Lee, H. Cheong, Phys. Rev. B 83 (2011) 081419.
[25] D.L. Nika, E.P. Pokatilov, A.S. Askerov, A.A. Balandin, Phys. Rev. B 79 (2009) 155413.
[26] P.G. Klemens, J. Wide Bandgap Mater. 7 (2000) 332.
[27] P.G. Klemens, Int. J. Thermophys. 22 (2001) 265.
[28] L. Lindsay, D.A. Broido, N. Mingo, Phys. Rev. B 83 (2011) 235428.